# PHYSICAL SIMULATION OF HIGH-RESOLUTION SATELLITE IMAGES FOR FRACTAL CLOUD MODELS

A. MARSHAK,[a] A. DAVIS,[a] R. CAHALAN, AND W. WISCOMBE

*NASA – Goddard Space Flight Center, Climate & Radiation Branch, Greenbelt, MD 20771, USA*

Based on fractal models for the horizontal distribution of cloud density, Landsat-type (i.e., 30 m resolution) radiance fields were simulated within the Nonlocal Independent Pixel Approximation (NIPA), an improved version of the Independent Pixel Approximation (IPA) that uses only the local optical thickness. Scale-by-scale analyses of liquid water variability inside stratus clouds indicate scale-invariance over three decades, from ≈10 m to ≈10 km. A simple two-parameter fractal cascade model reproduces the observed variability, thus capturing the rich turbulent structure in cloud density, hence optical thickness. IPA-based radiation fields of these models preserve scaling properties of fractal cloud models, at least for small moments; however Landsat cloud scenes show a characteristic scale (200–300 m) below which radiance fluctuations are much smaller. This is shown to be the effect of physical smoothing by horizontal photon transport. As a convolution of IPA field with gamma-type smoothing kernel, NIPA emulates this radiative smoothing and produces realistic Landsat-type images. Their statistical verisimilitude is checked with multifractal analyses. The simulations are graphically illustrated and compared with a real Landsat scene.

## 1 Introduction

Although it is well-recognized that clouds vary horizontally, most radiative transfer calculations for clouds in atmospheric dynamical simulation models still assume horizontal homogeneity. Suffering from a lack of data on cloud properties, the hope has been that these variations are unimportant for the bulk radiative properties. However, not only mean optical depth but also its spatial distribution affects cloud radiative properties.[1,2]

By the mid-1980's the fractal nature of cloud shapes became clear.[3] It is also well known that turbulence produces fractal structures. Together, these facts suggest that cloud internal structure can be simulated with fractal models. Indeed, the fractal cascade models[4,5] simulate the horizontal variability of liquid water observed in marine stratocumulus (Sc) clouds.[6,7] Power-law behavior of its energy spectrum,

$$E(k) \propto k^{-\beta}, \; k = 1/r \tag{1}$$

is valid over a large range of scales $r \approx 1/k$, from several meters to tens of kilometers; spectral exponent $\beta$ ranges from 1 to 2.

For inhomogeneous clouds, the "Independent Pixel Approximation" (IPA) calculates the radiation properties of each pixel using 1D plane-parallel radiative transfer theory.[8] Although IPA is a nonlinear transformation, to a first approximation, it preservers the scaling properties found in cloud models. However, recent analyses of Landsat cloud images of marine Sc[6,9,10] showed that, while the fluctuations of the radiance field follow those of cloud liquid water at large scales, at small scales, they exhibit much smoother

---

[a] Also Science Systems and Applications, Inc. (SSAI), 5900 Princess Garden Parkway, Lanham, MD 20706, USA

behavior. Hence a scale break in the radiance energy spectrum was found, meaning that there is a characteristic scale that separates two distinct scaling behaviors. As a result, IPA describes well the large-scale fluctuations of radiances, but overestimates them at small scales.

The shortcoming of IPA for small scales comes from the fact that while using plane-parallel radiative transfer theory locally, it ignores net horizontal photon transport. In order to simulate Landsat imagery down to very small scales and improve IPA without resorting to costly Monte Carlo (MC) schemes, we use a so-called "Nonlocal Independent Pixel Approximation" (NIPA) which, in empirical way, accounts for photon horizontal fluxes.
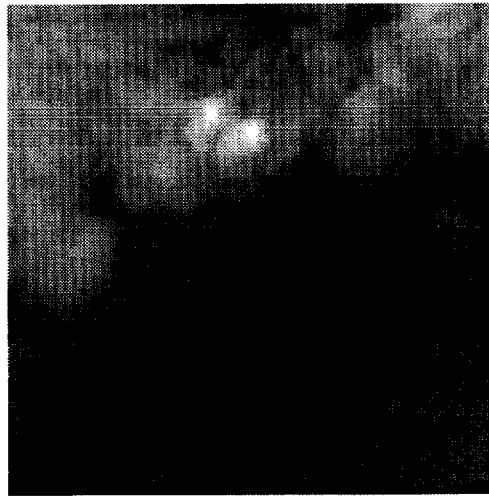


**Fig. 1** *Portion of a Landsat image in channel 2 (0.52–0.60 μm).* This $4\times4$ km$^2$ marine Sc scene was captured at $\ell$ = 30 m resolution off the coast of San Diego (Ca). For the whole image, about 7% of the pixels are saturated at gray-level 255.

## 2 Landsat Radiances

### 2.1 Wavenumber spectrum

Figure 1 is a typical Landsat cloud scene, a $4\times4$ km$^2$ portion of a Thematic Map image, $128\times128$ pixels. It was captured June 30, 1987, during the First ISCCP Regional Experiment (FIRE) and clearly illustrates the intricate structure of a marine Sc deck that extends far beyond this area.

Marine Sc is arguably the closest cloud–type to a horizontally homogeneous layer. Sc clouds are typically 300 m thick and 1000 km more across. Their mean optical thickness is $\approx$10–15, and frequently their cloud fraction approaches 100%; hence we will focus on their internal structure, assuming no gaps, over a range of scales from $\approx$10 m to $\approx$10–20 km.

The first scaling analysis of Landsat data performed in Ref. 6. Figure 2a shows a 2D energy spectrum $E(k)$ plotted against wavenumber $k$ in log-log axes. By using over $4\times10^6$ data points, the statistical noise is low enough that we can see at least two distinct

scale-breaks: one at 0.2–0.4 km, and one at $\approx$20 km. Between these two limits, power-law behavior prevails with an exponent $\beta \approx 2$ in Eq. (1). This two order of magnitude range of scale-invariance indicates the fractal nature of clouds. Studies[11] based on multiple instruments show that the scale-break at 20 km is not robust but the one at 200–400 m is.

The transition at scales 0.2–0.4 km to smoother behavior has a special interest; we will discuss it in details in Section 5. Here we only note that this scale-break is due to radiative smoothing and we will call it the "radiative smoothing scale." Because of the resolution of Landsat images ($\approx$ 0.03 km), we do not have enough scales below 0.2 km; thus the question about small-scale fractal structure of Landsat radiances remains open.



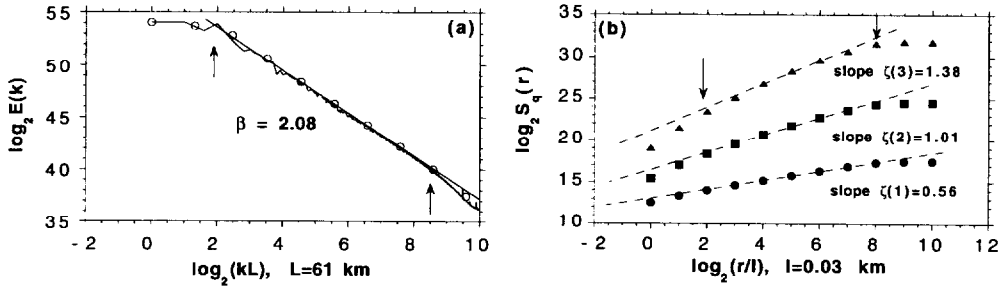**Fig. 2** *Energy spectrum and structure functions of the $61\times61$ km$^2$ radiance field, a portion of which is in Fig. 1.* Arrows indicate the characteristic scales. **(a)** $E(k)$ was averaged over 2048 columns for $r = 1/k$ going from $2\ell = 60$ m to $L = 2048\ell \approx 61$ km. The scale-break is clearly seen at $r \approx 100–200$ m. The dots correspond to octave-wide bins in $k$. **(b)** $S_q(r)$ ($q=1$, 2, and 3) was averaged over 2048 columns for 11 values of $r$, from $\ell = 30$ m to $2048\ell \approx 61$ km by factors of 2.

## 2.2 Structure functions

The robust feature of scale-invariance between $\approx$0.2 km and $\approx$20 km can be also apprehended in physical space. Let $\varphi(x) \in [0,255]$ be the gray-scale value, approximately proportional to nadir-viewing radiance, of the Landsat pixel at $x = (x_1,x_2) \in [0,L-1]\otimes[0,L-1]$ where we adopt a unit of length with pixel size $\ell = 1$; thus $L = 2048$.

In statistically isotropic situations, the "structure functions" $\langle[\varphi(x+r)-\varphi(x)]^q\rangle$ are functions of $r = |r|$ alone, and we can write

$$S_q(r) = \langle[\varphi(x+r)-\varphi(x)]^q\rangle \sim r^{\zeta(q)}, \quad q \geq 0. \quad (2)$$

The extension of this statistic for $q < 0$ is discussed in Ref. 12. Note that the function $S_2(r)$ is related to $E(k)$ by a Wiener–Khinchin theorem:

$$\zeta(2) = \beta{-}1. \quad (3)$$

Another special exponent is

$$H_1 = \zeta(1) \geq 0 \quad (4)$$

which is called the "roughness" or Hurst exponent; it varies from zero to unity.

Some general statements can be made about $S_q(r)$ and $\zeta(q)$ as functions of $q$. First, proper normalization in (2) requires $\zeta(0) = 0$. Furthermore, $\zeta(q)$ is a convex function[13]

and it is also non-decreasing if its increments are bounded[14,15]. For narrowly distributed increments, i.e., $S_q(r) \approx S_1(r)^q$, Eq. (2) yields

$$\zeta(q) = qH_1; \tag{5}$$

a single exponent $H_1$ determines the scaling of all the statistical moments of the increments. This is a characterizing property of fractional Brownian motion (fBm)[16].

We have computed $S_q(r)$ for $r/\ell = 1, 2, 4, \ldots, 2048$ where $\ell = 30$ m using the same data as for Fig. 2a. The range of moments $q$ is from 1 to 5 with increments of 0.2. Figure 2b illustrates the scaling properties of $S_q(r)$ for $q = 1, 2$ and 3. These curves reproduce 1D structure functions averaged over 2048 lines. Similar to the energy spectrum, we see two scale breaks: the transition to stationary behavior (slopes $\approx 0$), and the transition to smooth behavior at small scales that we will return to in Section 5.

In Fig. 3, $\zeta(q)$ for the Landsat radiances is easily distinguishable from that of fBm in Eq. (5) with the same $H_1 \approx 0.56$. However, we cannot rule out statistical compatibility of fBm and the radiance fields until finite sampling and finite size-effects are examined. The later are incorporated in the analysis presented in Ref. 17 showing that the radiance field is, at best, weakly multifractal in comparison with the definite multifractality of the cloud models described in the next section, and the observed[18] internal structure of marine Sc on which they are based.

## 3 Scale-Invariant Cloud Models

In this section we use stochastic models to simulate the natural fluctuations of cloud optical depth. The analyses of liquid water content (LWC) fluctuations inside marine Sc during FIRE and ASTEX (Atlantic Stratocumulus Transition Experiment) support scale-invariant models that obey power-law statistics over at least three orders of magnitude in scale.[7,18]

Starting with a homogeneous slab of length $L$, one can build a mass-conserving model by transferring a fraction $f_1$ of the mass from one half to the other in a randomly chosen direction. This is equivalent to multiplying the originally uniform density field on either side by factors $W_1^{(\pm)} = 1 \pm f_1$. The same procedure is repeated recursively at ever smaller scales, with fractions $f_i$, $i \geq 2$.

### 3.1 Singular Cascades

We now parameterize the multiplicative weights as

$$W_i^{(\pm)} = 1 \pm (1-2p) = \left\{ \begin{array}{c} 2p \\ 2(1-p) \end{array} \right\}, \ 0 \leq p < 1/2, \ i = 1, 2, \ldots, \tag{6}$$

independently of $i$, with 50/50 probability for the signs. This leads to the multifractal "$p$--model"[19] $\varepsilon(x)$ where $p$ directly controls the degree of concentration at each cascade step. The spectral exponent defined in $E_\varepsilon(k) \sim k^{-\beta_\varepsilon}$, $k > 0$, is

$$0 \leq \beta_\varepsilon(p) = 1 - \log_2[\ 1 + (1-2p)^2\ ] < 1. \tag{7}$$

Singular cascade models $\varepsilon(x)$ have interesting intermittency properties but their spectra with, $\beta_\varepsilon < 1$, do not scale as observed optical depth fields $\tau(x)$ that invariably have $\beta_\tau > 1$.

### 3.2 Bounded Cascades

A simple way to obtain $\beta_\tau > 1$ is to reduce the variance of the multiplicative weights in Eq. (6) at each cascade step. Taking

$$W_i^{(\pm)} = 1 \pm (1-2p)r_{i-1}{}^H, \; 0 \le p < 1/2, \; H > 0, \; r_i = L/2^i. \qquad (8)$$

leads to "bounded" cascade models.[5] The limit $H \to \infty$ yields a single jump (Heaviside step) from $2p$ to $2(1-p)$ at $x = L/2$.

By reducing the size of the jumps as the scale decreases, we are introducing a degree of continuity into the model. As a result, its spectral exponents moved into the range

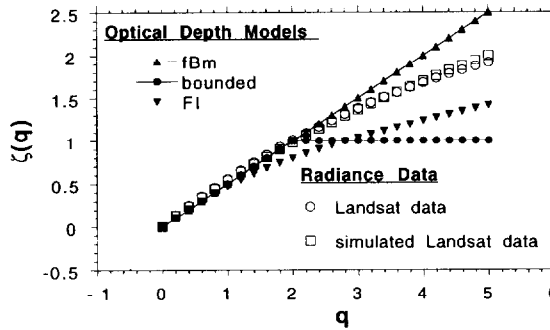$$1 < \beta_\tau(H) = \min\{2H,1\} + 1 \le 2, \qquad (9)$$

independently of $p$.



**Fig. 3** *Comparison of exponent functions* $\zeta(q)$. Two nadir radiance fields: Landsat data (scale range between 0.1–0.2 km and 10–20 km) and IPA-simulated Landsat data with fractionally integrated (FI) cascade model of optical depth (all scales involved). Bold dots represent cloud optical depth models: fBm ($H = 0.5$), bounded ($H = 0.5$) and FI ($p = 0.32$ and $H^* = 0.54$) models. Both fBm and bounded models show theoretical results, the rest are numerically obtained.

In the limit of infinite number of cascades, the bounded model has[15]

$$\zeta(q) = \begin{cases} qH, & 0 \le q \le 1/H \\ 1, & 1/H \le q \le \infty \end{cases} ; \qquad (10)$$

so Eq. (9) follows from Eqs. (3) and (10). Thus the bounded cascade model, while multifractal, cannot be distinguished from monoscaling fBm for moments smaller than $q = 1/H$.

To summarize, bounded model is a well-studied tutorial model of horizontal inhomogeneity of cloud optical thickness. To a first approximation, it reproduces lower order statistical moments of cloud liquid water distribution. However, as follows from Eq. (10), its $\zeta(q) \le 1$ whereas[18] the higher-order moments of LWC fluctuations

substantially exceed unity. In the next subsection we describe another model, fractionally integrated cascades[4], that overcomes this limitation.

### 3.3 Fractional Integration

Another way of transforming the situation described in Section 3.1 (singular cascades with $\beta_\varepsilon < 1$) into a more realistic one ($\beta_\tau > 1$) is power-law filtering in Fourier space[4]; this will bring the spectral exponent to any prescribed value. In particular, we have

$$\beta_\tau(p,H^*) = \beta_\varepsilon(p) + 2H^* \tag{11}$$

where $H^*$ describes the low-pass filter in $k^{-H^*}$. In physical space, this operation —also known as "fractional integration" (FI)— is a convolution with a weakly singular kernel.

In contrast to the bounded model, we are unable to derive analytically structure function exponents for FI model for all values of $q$. Instead, we simulated nine 2D cascades and the associated FI models with $p = 0.32$ ($\beta_\varepsilon = 0.82$) and $H^* = 0.54$, which according to Eqs. (7) and (11) yields $\beta_\tau = 1.9$. Structure functions $S_q(r)$ are computed numerically for each stripe and estimated over all $2^9 = 512$ stripes. To demonstrate scaling behavior of FI model, the first three moments of $S_q(r)$ vs. scale $r$ are plotted in Fig. 4. We see that slopes representing $\zeta(q)$ ($q$=1, 2 and 3) increase nonlinearly. This is an indication of the multifractal origin of this model.
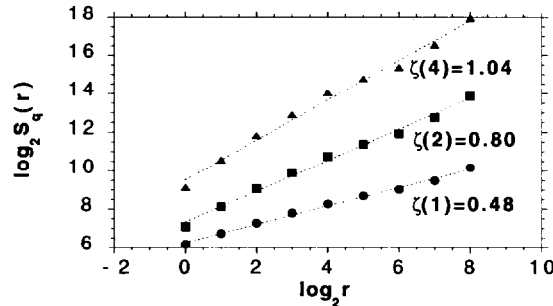


**Fig. 4** *Structure functions $S_q(r)$ ($q$=1, 2, and 3) for the fractionally integrated cascade model.*

To compare three models (monofractal fBm and two multifractal models: bounded and FI), we plotted their structure functions $S_q(r)$ in Fig. 3 for $q$ from 0 to 5 with 0.2 increments. As we see, the bounded model is the "most multifractal" among them since its $\zeta(q)$ is the most nonlinear. With at least one more tunable parameter than bounded cascades, FI cascades are better candidates for simulating observed liquid water fluctuations.[10,18]

In the next section we briefly discuss the simplest radiative transfer method that can treat horizontally inhomogeneous cloud structure; we apply it to the FI cascade model described above.

## 4   Simple Radiative Transfer

The simplest way of treating radiative transfer in a horizontally inhomogeneous cloud model is to use an "Independent Pixel Approximation" or IPA.[5] This amounts to

applying plane-parallel theory on a per pixel basis. In other words, the IPA ignores any net horizontal photon transport. As a result, the domain-averaged of plane-parallel radiances, $\langle R_{PP}(\tau) \rangle$, depends only on the one-point probability distribution of the optical depth field. To compute $R_{PP}$, one can use any general purpose plane-parallel radiative transfer code.

Since radiance $R_{PP}$ is a convex function[5], Jensen's inequality[20] states that $\langle R_{PP}(\tau) \rangle$ $\leq R_{PP}(\langle \tau \rangle)$, i.e., the domain-averaged plane-parallel reflectivity is larger than its IPA counterpart. The difference between left and right parts in the above inequality is called "plane-parallel bias".[8] For typical marine Sc albedos, the bias is about 15%; this means that in order to obtain the correct albedo from a plane-parallel model, 30% less liquid water must be used.
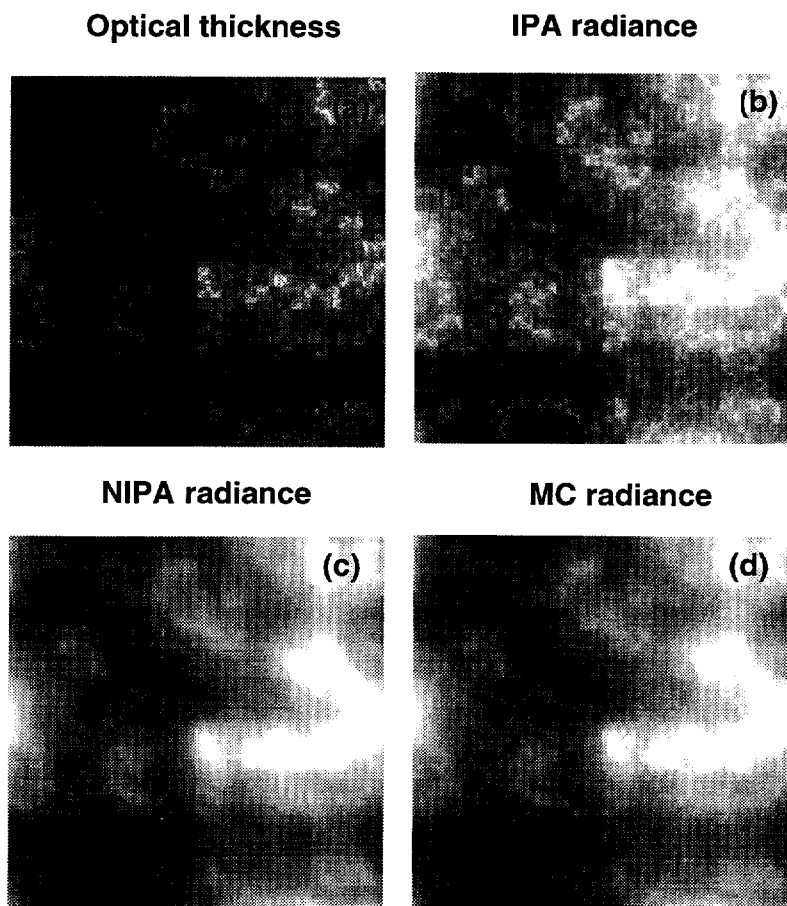
**Optical thickness**       **IPA radiance**



**NIPA radiance**       **MC radiance**



**Fig. 5** *2D optical thickness and nadir radiance fields.* (*a*) Density plot of the optical thickness simulated by FI model ($p = 0.32$ and $H^* = 0.54$). The dense regions are white, the least dense regions black. The shade of gray is linearly proportional to the pixel value. Optical thickness varies from 4 to 43. (*b*) $R_{IP}$ for sun at 22.5° and a photon-scattering kernel with an asymmetry factor $g = 0.85$. The cloud is illuminated from the top of the image. Cloud geometrical thickness $h = 300$ m and the horizontal grid size is 128×128 with 30-m pixels. The gray color range is from 55 (black) to 255 (white). (*c*) $R_{NIP}$ for the same conditions as in panel *b* . The gray scale range is the same as panel *b*. (*d*) $R_{MC}$ for the same conditions as in panel *b* . The gray color scale is the same as in panel *b*.

From the other side, using Monte Carlo (MC) results as a standard of comparison, it is shown[5] that the IPA is very accurate for large-scale averages in the case of Sc clouds with internal LWC fluctuations modeled with bounded cascades. The same is true for FI models of cloud liquid water.

Figure 5b shows a nadir radiance field of equal size and resolution as the one of Landsat in Fig. 1; however, it does not have the scale-break at 0.1–0.2 km. The radiances were computed by IPA applied to FI model of cloud optical thickness (Fig. 5a) on a pixel-by-pixel basis. (To better simulate Landsat measurements, we first found a threshold that yields the same fraction of saturated pixels as in a Landsat cloud scene and then set to this threshold all IPA radiances which exceeded it; next we digitized the results on 255 levels.)

Parameters $p$ and $H^*$ of FI model were chosen in such a way that the hierarchy of structure function exponents $\zeta(q)$ of (saturated and digitized) IPA radiances matches those of Landsat. We can see that two curves in Fig. 3 are almost identical for moments up to order 5. It is interesting to notice that there is not much difference in $\zeta(q)$ between cloud models and IPA radiances for moments smaller than about 1.5. Indeed, because of the continuity property of the random field $\tau$, for small enough moments we have

$$|\Delta R_{\mathrm{IP}}|^q \sim J\,|\Delta\tau|^q \qquad (12)$$

where is $J$ is the Jacobian of $R$ vs. $\tau$ which is bounded. This argument however fails for higher-order structure functions.[9,10]

In the next section we show how to improve the IPA based simulations of Landsat cloud scenes. We will use interpixel radiative corrections which yield much smaller fluctuations of radiances on scales below the radiative smoothing scale.

## 5   Small-Scale Corrections

As we could see in Figs. 2a and 2b, there is a transition to smoother behavior around 0.1–0.2 km: both energy spectra and structure functions show steeper slopes for small scales. This scale-break is due to the radiative smoothing effect of multiply-scattered photons[9,10]; thus the characteristic transition scale has been called "radiative smoothing scale." Using the diffusion approximation, the radiative smoothing scale $\eta$ is the harmonic mean between photon transport mean free path and geometrical cloud thickness. This can be written as

$$\eta \approx h[(1-g)\langle\tau\rangle]^{-1/2}, \qquad (13)$$

where $h$ and $\langle\tau\rangle$ are respectively geometrical and (mean) optical cloud thickness, and $g$ is the asymmetry factor. For typical marine Sc[6], $h = 0.3$ km, $\langle\tau\rangle = 13$, and $g = 0.85$; Eq. (13) then yields $\eta \approx 0.22$ km which is consistent with those observed in Figs. 2a and 2b.

Next, studying numerically the distribution of the "spot" of reflected light associated with a point-wise source (essentially the cloud's radiative Green function), it was found[9] that the spot can be well approximated by a two-parameter gamma-type distribution,

$$P(\alpha,\eta\,;x) = c\,(x_1{}^2 + x_2{}^2)^{(\alpha-1)/2}\exp\left(-\frac{(x_1{}^2 + x_2{}^2)^{1/2}}{\eta}\right), \quad \alpha > 0, \eta > 0 \qquad (14)$$

where $c$ is a normalization constant and $x = (x_1, x_2)$. In addition to parameter $\eta$ defined in Eq. (13), we have a parameter $\alpha = \langle x \rangle^2 / (\langle x^2 \rangle - \langle x \rangle^2)$, which can be estimated numerically. Note that, while $\eta$ defines the scale-break, $\alpha$ determines the behavior of scales smaller than $\eta$. For nadir radiance in marine Sc type clouds, $\alpha \approx 0.5$.[9]

Finally, to improve IPA for small scales we use a convolution of the IPA radiance field with the gamma-type smoothing kernel in Eq. (14),

$$R_{NIP}(x) = P(\alpha, \eta; x) * R_{IP}(x). \qquad (15)$$

One can show[9] that for scales larger than $\eta$ energy spectra $E(k)$ of $R_{NIP}$ and $R_{IP}$ are alike; however small-scale spectrum of $R_{NIP}$ has much steeper slope which is defined by $\alpha$, $\eta$, and the original slope.

Figure 5c shows $R_{NIP}$ radiance field which was computed in Fourier space using Eq. (15). As expected, fields in Figs. 5b and 5c have similar large-scale variability; the small scales in Fig. 5c however are much smoother. In contrast, Figs. 5c and 5d look much closer (in the later, we plotted the results of MC applied to cloud model in Fig. 5a). Note that the CPU time for the calculation of $R_{NIP}$ was about 5000 shorter than for $R_{MC}$!

## 6 Summary

We used both structure functions and energy spectra to analyze Landsat images of marine stratocumulus clouds. Good scaling from about 0.1–0.2 km to 10–20 km (Figs. 2a and 2b) indicates the fractal structure of the Landsat radiances and suggests the use of scale-invariant models to simulate horizontal distribution of cloud optical depth. Two two-parameter cascades models— bounded[5,8] and fractionally integrated[4,17]—were chosen to simulate cloud structure. Both of them are stochastically continuous and have a spectral exponent $\beta_\tau > 1$. Structure-function analysis of bounded cascades yield[15] $\zeta(q) \leq 1$. As this is not the case for real clouds[18], a more flexible fractionally integrated cascade model has been used for the radiation field calculations.

The simplest radiative transfer technique to treat cloud horizontal inhomogeneity is the "Independent Pixel Approximation" (IPA) which uses standard plane-parallel theory but on a pixel-by-pixel basis. Since IPA preserves scale-invariance of cloud structure, the resulting radiation field (Fig. 5b) does not have any characteristic scale and its structure functions exhibit straight lines on a log-log plot for all scales. The $\zeta(q)$ of the IPA field is similar to the one of Landsat cloud scene *only for scales larger than* 0.1–0.2 km. For small scales, both Landsat (Fig. 1) and MC calculated radiance fields (Fig. 5d) show much smoother than the IPA field behavior; this is due to the radiative horizontal fluxes ignored by IPA.[9,10]

To improve IPA performance for small scales, the "Nonlocal" IPA (NIPA) was applied to a scale-invariant optical depth model. Unlike IPA, NIPA takes into account net horizontal transport; the large-scale fluctuations of NIPA are similar to those of IPA while the small-scale behavior is smoother and reproduces statistical properties observed in Landsat data and simulated with MC.[9] Two fields NIPA and MC are illustrated in Figs. 5c and 5d.

To summarize, Landsat cloud scenes simulated with NIPA applied to FI cascade models of cloud optical depth reproduce both scale-invariant structure of large-scale fluctuations and smooth behavior of small scales of observed Landsat images. This

conclusion is based on a scale-by-scale structure function analysis of both simulated and satellite-measured fields.

## Acknowledgments

## References

1. G.L. Stephens, *Mon. Wea. Rev.,* **113**, 1834 (1985).
2. G.L. Stephens, *J. Quant. Spectrosc. Radiat. Transfer,* **36**, 51 (1986).
3. S. Lovejoy, *Science,* **216**, 185 (1982).
4. D. Schertzer, and S. Lovejoy, *J. Geophys. Res.,* **92**, 9693 (1987).
5. R.F. Cahalan, W. Ridgway, W.J. Wiscombe, T.L. Bell, and J.B. Snider, *J. Atmos. Sci.,* **51**, 2434 (1994).
6. R.F. Cahalan and J.B. Snider, *Remote Sens. Environ.,* **28**, 95 (1989).
7. A. Davis, A. Marshak, W.J. Wiscombe, and R.F. Cahalan, *J. Atmos. Sci.,* **53**, 1538 (1996).
8. R.F. Cahalan, *Nonlin. Proc. Geophys.,* **1**, 156 (1994).
9. A. Marshak, A. Davis, W.J. Wiscombe, and R.F. Cahalan, *J. Geophys. Res.,* **100**, 26247 (1995).
10. A. Davis, A. Marshak, R. Cahalan, and W. Wiscombe, *J. Atmos. Sci.,* **54** (1997).
11. S. Lovejoy, D. Schertzer, P. Silas, Y. Tessier, and D. Lavallée, *Ann. Geophysicae,* **11**, 119 (1993).
12. J.F. Muzy, E. Bacry, and A. Arnéodo, *Phys. Rev. E,* **47**, 875 (1993).
13. G. Parisi and U. Frisch, in *Turbulence and Predictability in Geophysical Fluid Dynamics,* eds. M. Ghil, R. Benzi, and G. Parisi, (North Holland, Amsterdam, 1985) p. 84.
14. U. Frisch, *Proc. R. Soc. Lond. A,* **434**, 89 (1991).
15. A. Marshak, A. Davis, R. Cahalan, and W. Wiscombe, *Phys. Rev. E,* **49**, 55 (1994).
16. B.B. Mandelbrot, *Fractals: Form, Chance, and Dimension* (W.H. Freeman and Co., San Francisco, 1977).
17. A. Davis, A. Marshak, W. Wiscombe, and R. Cahalan, in *Current Topics in Nonstationary Analysis*; eds. G. Trevino, J. Hardin, B. Douglas, and E. Andreas, (World-Scientific, Singapore, 1996) pp. 97.
18. A. Davis, A. Marshak, W.J. Wiscombe, and R.F. Cahalan, *J. Geophys. Res.,* **99**, 8055 (1994).
19. C. Meneveau, and K.R. Sreenivasan, *Phys. Review Lett.,* **59**, 1424 (1987).
20. J.L.W.V. Jensen, *Acta Math.,* **30**, 789 (1906).